JCTC Journal of Chemical Theory and Computation

Magnetostructural Dynamics with the Extended Broken Symmetry Formalism: Antiferromagnetic [2Fe-2S] Complexes

Nisanth N. Nair,* Eduard Schreiner,† Rodolphe Pollet,‡ Volker Staemmler, and Dominik Marx

Lehrstuhl für Theoretische Chemie, Ruhr-Universität Bochum, 44780 Bochum, Germany

Received March 13, 2008

Abstract: A general spin-projection framework is laid out which allows one to perform ab initio molecular dynamics simulations of antiferromagnetically coupled spin dimers. The method extends the well-established broken-symmetry formalism and is systematically and consistently improvable. It allows for accessing structure within the same spin-projection approximation as employed to compute the exchange coupling constant J of such complexes in their low-spin state as a function of time. The resulting time evolution of the exchange coupling, $J(t)$, can be analyzed most conveniently in terms of the corresponding power spectrum, $J(\omega)$, thus giving access to dynamical magnetostructural properties. The method has been implemented using a well-tested approximation to spin-projection and was applied to a minimal [2Fe-2S] model, i.e. to the $[Fe_2S_2(SH)_4]^{2-}$ complex at 300 K in vacuo. Thermal fluctuations at room temperature are found to change the antiferromagnetic coupling J by about 50% with respect to the average value, and the features of its power spectrum, $J(\omega)$, can be traced back to a coupling of J to particular vibrational modes.

1. Introduction

There is a vast amount of literature on the computation of exchange coupling constants in bi- and polynuclear transition metal complexes using both wave function-based and density-based methods.[1–9] Part of this interest is stimulated by the crucial importance of magnetically coupled transition metal centers in metalloproteins, such as nonheme iron proteins.[10–13] In particular, in iron−sulfur proteins prosthetic groups of the type [*n*Fe-*m*S] consist of a varying number of iron centers and sulfur atoms that are bridging the iron centers. In addition, the [*n*Fe-*m*S] complexes are bound to the backbone by sulfur atoms typically belonging to cysteine residues or by nitrogen atoms from histidines in the case of Rieske proteins. By virtue of the different oxidation states of the iron sites such cofactors serve as electron transfer relays and catalytic redox agents not only in bacteria but also in plants and higher animals.[10–13] Thus, particular combinations of oxidized (ferric) Fe(III) and reduced (ferrous) Fe(II) sites can establish different total oxidation states in a given biomolecular environment. In addition to tunable oxidation states, the magnetic structure can be rather involved, as the individual iron centers typically prefer a high-spin (HS) state, $S_{Fe} = 5/2$, in the oxidized state with a formal charge of +3 and a d^5 configuration.

A particularly important and well-studied family is the fully oxidized ferredoxin where the two HS metal centers in the inorganic [2Fe-2S] complex are magnetically coupled. This magnetic system consists of two paramagnetic transition metal centers, Fe^{3+}, both of which have an equal number of electrons, bridged by two diamagnetic centers, S^{2-}. In the ground state, the local spins at the metal sites are antiferromagnetically coupled to an overall low-spin (LS) state of this homovalent binuclear core.[14,15] To understand the

* Corresponding author e-mail: nisanth.nair@theochem.ruhr-uni-bochum.de.

† Present address: Theoretical and Computational Biophysics Group, Beckman Institute, Urbana, IL 61801.

‡ Permanent address: Laboratoire Francis Perrin, Commissariat a l'Énergie Atomique, 91191 Gif-sur-Yvette, France.

10.1021/ct800089x CCC: $40.75
Published on Web 06/26/2008

antiferromagnetic coupling it is worth looking at the exchange interactions between the two metal centers.[16–20] The two sites can interact either by "direct" exchange or by "superexchange". Direct exchange is a through-space interaction depending on the direct overlap of the orbitals at the two metal centers. It decays exponentially with the metal−metal distance and causes always a ferromagnetic alignment. Superexchange, on the other hand, is mediated through a diamagnetic bridge and yields antiferromagnetic coupling in most cases.

Two complementary pictures are frequently involved to explain the physical origin of superexchange.[4] In the Anderson model,[17,18] one assumes that an electron is hopping from one metal center to the other through the diamagnetic bridge. In the HS case, in which all unpaired electrons on the two metals have the same spin, such hopping is not possible because all orbitals with this spin are already occupied. However, in states with lower spin, this hopping leads to a lowering of the energy, thus to an antiferromagnetic coupling. The theoretical description of this effect requires the inclusion of "charge transfer" excitations, i.e. in our system $d^5d^5 \rightarrow d^4d^6$ excitations.[10,21] On the other hand, in the Kahn model,[22] one uses wave functions in which the partially occupied orbitals at the two metal centers, the "magnetic orbitals", are allowed to be nonorthogonal. They can be delocalized and overlap at the diamagnetic bridge. Again, in the HS state the Pauli exclusion principle prevents this overlap, but in states with lower spin it reduces the energy and leads to an antiferromagnetic coupling. Both models have in common that the strength of the superexchange coupling, i.e. the exchange coupling constant J, depends sensitively on the distance between the metal and the bridging atom in the "exchange pathway" as well as on the metal-bridge-metal angle.[19,20,23]

Accurate treatments of the true multireference nature of such antiferromagnetically coupled LS ground states require, in principle, sophisticated electronic structure methods.[5–9,19] A much simpler approach is to use a single-determinant spin-polarized (unrestricted) representation to describe their electronic structure, usually referred to as the broken-symmetry (BS) determinant, which describes an electronic configuration with unpaired electrons localized mainly on the two transition metal centers. A clear discussion of the physical content of such BS single-determinant wave functions can be found in ref 21. Obviously, the BS state does not represent the true antiferromagnetic ground state.[24,25] Moreover, this state features spin contamination since it is not an eigenstate of the total spin operator. Thus, using a single BS determinant imposes a severe approximation, although it can be used straightforwardly in the framework of ab initio molecular dynamics (AIMD) to take fluctuation effects into account.

Sophisticated quantum-chemical methods, which can be employed to correctly treat the multireference character of the ground-state wave function,[5–9,23,26] however impose severe limitations on the systems that are accessible and the questions that can be addressed. A viable alternative is to have recourse to exact[26,27] or approximate[29–31] spin-projection schemes, which offer a compromise in terms of cost versus accuracy and allow the calculation of the exchange coupling constant J directly. They rely on an approximate purification of the spin state[24,32] by carrying out *independent* total energy calculations for several spin configurations.[1,33] Such schemes have proven to perform particularly well to compute exchange coupling constants for binuclear homovalent complexes in static electronic structure calculations.[34–37]

Here, we extend the idea of using a two-determinant spin-projection technique formulated in a generalized framework, which is suitable for describing the antiferromagnetic coupling of homovalent binuclear iron complexes. In particular, this ansatz is the basis for implementing multideterminant Car−Parrinello AIMD techniques thus yielding the extended broken-symmetry (EBS) scheme. The EBS method allows one to investigate the interplay of structural changes and magnetic properties at finite temperature, thus extending the Goodenough-Kanamori rules[38–40] from the static limit to unconstrained dynamics. Along this line of thinking about magnetic interactions, a very useful tool is to analyze the power spectrum, $J(\omega)$, obtained from the dynamical evolution, $J(t)$, of the exchange coupling constant, J, that is computed "on the fly" along the EBS AIMD trajectories. A particular version of this scheme has already been applied to analyze the dynamical magnetostructural properties of a specific ferredoxin in the framework of a QM/MM generalization,[41] where the interplay between magnetic dynamics and vibrational/configurational motion can be understood in terms of $J(\omega)$.

2. Methodology

2.1. Getting Started: Heisenberg Model. On a phenomenological level the exchange coupling in homovalent magnetic dimers may be modeled by the Heisenberg (or Heisenberg−Dirac-van Vleck) spin Hamiltonian[42–44]

$$\hat{H} = -2J\hat{S}_A\hat{S}_B \tag{1}$$

where $\hat{S}_A$ and $\hat{S}_B$ are effective local spin operators at the two sites A and B, respectively. Usually, J is referred to as the exchange (magnetic) coupling constant between the two paramagnetic centers and the sign is taken in such a way that $J > 0$ implies ferromagnetic coupling, whereas $J < 0$ describes antiferromagnetic or ferrimagnetic coupling.

Defining the total (coupled) spin operator $\hat{S}$ in terms of the local spin operators $\hat{S}_A$ and $\hat{S}_B$

$$\hat{S} = \hat{S}_A + \hat{S}_B \tag{2}$$

the Hamiltonian (1) may be rewritten[45] as

$$\hat{H} = -J(\hat{S}^2 - \hat{S}_A^2 - \hat{S}_B^2) \tag{3}$$

and hence the energy of a pure spin state is in general given by

$$E^S = -J[\langle\hat{S}^2\rangle^S - \langle\hat{S}_A^2\rangle - \langle\hat{S}_B^2\rangle] = -J[S(S+1) - S_A(S_A+1) - S_B(S_B+1)] \tag{4}$$

where $S \in [S_{min}, S_{max}]$ is the total spin quantum number of the coupled system; S_A and S_B are the local spin quantum numbers, which are kept fixed for the sites A and B. Thus,

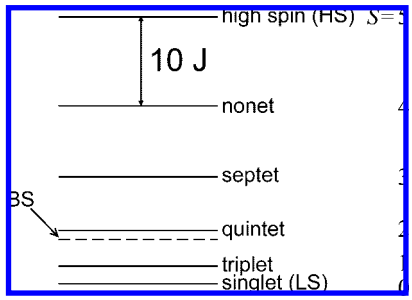

Figure 1. Sketch of a spin-ladder generated by Heisenberg's spin Hamiltonian (eq 1) for a d^5-d^5 binuclear system with an antiferromagnetic coupling. The position of the BS state within the ladder is indicated by the dashed line. Note: the BS state is not the $S = 0$ antiferromagnetic LS eigenstate of the coupled spins.

Hamiltonian (1) generates Heisenberg's spin-ladder of eigenstates (see Figure 1) with total spins S in the range from $S_{min} = |S_A - S_B|$ (low-spin, LS) to $S_{max} = S_A + S_B$ (high-spin, HS).

Thus, for given fixed local spin quantum numbers S_A and S_B at the two sites, eq 4 gives rise to Landé's interval rule

$$E^S - E^{S-1} = -2JS \tag{5}$$

which allows one to calculate the exchange coupling constant J knowing the energies of only two states, E^S and E^{S-1}. Moreover, it creates the possibility to access the energies of *all* spin states in the ladder (see Figure 1) if J and the total energy of *one* state is known. To calculate these quantities one needs the Clebsch-Gordan-coupled spin eigenstates $|S_A S_B; SM\rangle$ of the employed many-electron Hamiltonian. On the one hand, these exact spin eigenstates are not easily accessible computationally for many-electron systems such as molecular complexes or solids in the framework of realistic total energy electronic structure calculations. On the other hand, it appears viable to evaluate the expectation value $\langle \hat{S}^2 \rangle^S$ of the total spin operator in the total energy expression

$$E^S = -J[\langle \hat{S}^2 \rangle^S - S_A(S_A + 1) - S_B(S_B + 1)] \tag{6}$$

using approximately coupled states as obtained by approximate electronic structure calculations. Importantly, this will yield access, via eq 5, not only to J itself but also to any coupled state of the entire spin-ladder if only one of its states is known.

2.2. The Broken Symmetry Approach to *J*. In particular, the high-spin (HS) and broken-symmetry (BS) states may be used to estimate the coupling constant J using eq 6 in conjunction with Landé's rule.[28,29,45] The total energies of the S = HS and the S = BS states, i.e. E^{HS} and E^{BS}, are given by

$$E^{HS/BS} = -J[\langle \hat{S}^2 \rangle^{HS/BS} - S_A(S_A + 1) - S_B(S_B + 1)] \tag{7}$$

and can be easily calculated using a single Slater or Kohn−Sham (KS) spin-polarized (unrestricted) determinant. Here, it is assumed that the considered state is an eigenstate of the local $\hat{S}_A^2$ and $\hat{S}_B^2$ operators. From eq 7 it is clear that J can be readily expressed using the difference of the energies of the BS and HS states

$$J = \frac{E^{BS} - E^{HS}}{\langle \hat{S}^2 \rangle^{HS} - \langle \hat{S}^2 \rangle^{BS}} \tag{8}$$

which is the same formula written down earlier by Yamaguchi and co-workers.[46,47]

At this point it is necessary to address the role of the so-called "magnetic orbitals" in the calculation of the expectation value of the $\hat{S}^2$ operator.[21] Löwdin's formally *exact* expression[48] for the total spin of an n-electron system (with n^α and n^β spin-up and spin-down electrons respectively), i.e.

$$\langle \hat{S}^2 \rangle = -\frac{n(n-4)}{4} + \int \Gamma(\mathbf{r}_1\sigma_1, \mathbf{r}_2\sigma_2 | \mathbf{r}_1\sigma_2, \mathbf{r}_2\sigma_1) d\mathbf{x}_1 d\mathbf{x}_2 \tag{9}$$

where $\mathbf{x}_i = (\mathbf{r}_i, \sigma_i)$ is the combined spatial and spin coordinate of electron i and $\Gamma(\mathbf{r}_1\sigma_1, \mathbf{r}_2\sigma_2 | \mathbf{r}_1\sigma_2, \mathbf{r}_2\sigma_1)$ is the two-particle density matrix

$$\Gamma(\mathbf{x'}_1, \mathbf{x'}_2 | \mathbf{x}_1, \mathbf{x}_2) = \frac{n(n-1)}{2} \int \Psi^*(\mathbf{x'}_1, \mathbf{x'}_2, ..., \mathbf{x}_n) \times \Psi(\mathbf{x}_1, \mathbf{x}_2, ..., \mathbf{x}_n) d\mathbf{x}_3 ... d\mathbf{x}_n \tag{10}$$

can be rewritten in terms of off-diagonal elements of the two-particle density matrix[49]

$$\langle \hat{S}^2 \rangle = \left(\frac{n^\alpha - n^\beta}{2}\right)\left(\frac{n^\alpha - n^\beta}{2} + 1\right) + n^\beta + 2 \int \Gamma(\mathbf{r}_1\alpha, \mathbf{r}_2\beta | \mathbf{r}_1\beta, \mathbf{r}_2\alpha) d\mathbf{r}_1 d\mathbf{r}_2 \tag{11}$$

where $n^\alpha + n^\beta = n$, and it is assumed without loss of generality that $n^\alpha \geq n^\beta$.

In order to rewrite this equation in terms of local spin operators it is necessary to substitute $n^\alpha = n^\alpha_{mag} + n^\alpha_{nmag}$ and $n^\beta = n^\beta_{mag} + n^\beta_{nmag}$, where n^α_{mag} (n^β_{mag}) and n^α_{nmag} (n^β_{nmag}) is the number of unpaired and paired, i.e., "magnetic" and "non-magnetic" α (β) electrons, respectively. Since $n^\alpha_{nmag} = n^\beta_{nmag}$, eq 11 simplifies to

$$\langle \hat{S}^2 \rangle = \left(\frac{n^\alpha_{mag} - n^\beta_{mag}}{2}\right)\left(\frac{n^\alpha_{mag} - n^\beta_{mag}}{2} + 1\right) + n^\beta_{mag} + \Theta \tag{12}$$

where

$$\Theta = n^\beta_{nmag} + 2 \int \Gamma(\mathbf{r}_1\alpha, \mathbf{r}_2\beta | \mathbf{r}_1\beta, \mathbf{r}_2\alpha) d\mathbf{r}_1 d\mathbf{r}_2 \tag{13}$$

which is an exact expression that does not rely on any orbital picture.

In the BS state $n^\alpha_{mag} = 2S_A$ and $n^\beta_{mag} = 2S_B$, whereas for the HS state $n^\alpha_{mag} = 2(S_A + S_B)$ and $n^\beta_{mag} = 0$. Thus, eq 8 may be reformulated using the explicit expression for the total spin operators to obtain a general formula for the coupling constant J

$$J = \frac{E^{BS} - E^{HS}}{4S_A S_B - \Theta^{BS} + \Theta^{HS}} = \frac{E^{BS} - E^{HS}}{S^2_{max} - S^2_{min} - \Theta^{BS} + \Theta^{HS}} \tag{14}$$

based on two total energies E^{BS} and E^{HS} together with the corresponding terms Θ^{BS} and Θ^{HS}, respectively. Note, for

a pure spin state $|S_A S_B; SM\rangle$ one finds $\langle \hat{S}^2 \rangle^S = S(S+1)$, i.e., $\Theta = 0$, which makes clear the well-known point that Θ is a spin correction term.

In order to understand the physical meaning of the spin correction terms Θ^{HS} and Θ^{BS}, it is useful to consider the integral in eq 11 from the point of view of unrestricted Hartree−Fock (UHF) theory, i.e., within a convenient orbital picture.[24] In this one-determinantal orbital approximation Θ can be expressed for the HS and BS state as

$$\Theta_{UHF} = n^{\beta}_{nmag} - \sum_{i}^{m}\sum_{j}^{m} f_i^{\alpha} f_j^{\beta} \left| \int_{ij}^{\alpha\beta} \right|^2 \tag{15}$$

where $f_i^{\sigma} = \{0, 1\}$ denotes the occupation number of the HF spin orbital ψ_i^{σ}, m is the number of orbitals, and $\int_{ij}^{\alpha\beta} = \langle \psi_i^{\alpha} | \psi_j^{\beta} \rangle$ is the overlap matrix. For a closed shell case, when the spatial parts of the α and β parts are identical $|\int_{ij}^{\alpha\beta}| = \delta_{ij}$ and the double sum in eq 15 reduces to the number of occupied states, i.e. the number of paired electrons, such that the two terms in eq 15 cancel each other, and thus $\Theta = 0$.

For open shell cases the α and β electrons of the lower-lying closed shells do not occupy the same spatial orbitals, since the interactions are different between electrons with same spin and electrons with opposite spin. Therefore, to stay within the UHF picture, the double sum will yield less electrons than the total number of β electrons, which implies immediately that the expectation value of $\hat{S}^2$ will be larger than the exact one. This gives rise to spin contamination. In cases like the iron sulfur systems considered in this work, where there are two radical sites of same spin, the double sum takes care of the nonorthogonality of the doubly occupied orbital of α and β spins and the overlap of magnetic orbitals. Thus, Θ is a "correction term" and takes into account the spin contamination and the overlap of magnetic orbitals when $\langle \hat{S}^2 \rangle^{HS/BS}$ is evaluated in expressions like eq 8.

Having discussed the correction Θ in terms of the UHF approximation, it should be stressed that this term can be alternatively approximated in the framework of density functional theory following for instance ref 49. In particular, using the exchange-only homogeneous electron gas leads to the expression

$$\Theta_{LSD} = -\int' [\rho^{\alpha}(\mathbf{r}) - \rho^{\beta}(\mathbf{r})] d\mathbf{r} \tag{16}$$

in the spirit of the local spin density (LSD) approximation,[49] where the prime indicates that the integration is carried out only in those regions of space where the spin density is negative, i.e. for $[\rho^{\alpha}(\mathbf{r}) - \rho^{\beta}(\mathbf{r})] < 0$; the spin density can of course be computed using a density functional beyond the LSD approximation. Alternatively, one might just use the spin-polarized KS orbitals φ_i instead of the unrestricted HF orbitals ψ_i to compute the orbital overlap matrix $\int_{ij}^{\alpha\beta}$ in eq 15 leading to

$$\Theta_{nonint} = n^{\beta}_{nmag} - \sum_{i}^{m}\sum_{j}^{m} f_i^{\alpha} f_j^{\beta} \langle \varphi_i^{\alpha} | \varphi_j^{\beta} \rangle^2 \tag{17}$$

which yields an approximation in the spirit of the (fictitious) noninteracting KS reference system concept,[49] keeping in mind that the KS determinant is not the wave function of the (real) interacting many-electron system. Both density functional based approximations to $\langle \hat{S}^2 \rangle$, and thus to Θ in expressions such as eq 14, have been shown to perform reasonably well for a set of atoms and small open-shell molecules,[49] see also ref 50 for further assessment and development. It is mentioned in passing that this general idea is open to more sophisticated spin correction treatments, possibly in connection with more elaborate density functionals as e.g. addressed in refs 50 and 51 or by incorporating spin symmetry into the KS treatment as done in the spin-restricted ensemble-referenced KS method.[52–54]

In order to proceed, it is useful to consider various approximations to simplify Θ for the HS and BS states, which in turn will lead to corresponding approximations to eq 8 in order to estimate J. First of all, a useful approximation is to neglect Θ in the HS state, $\Theta^{HS} = 0$, since spin contamination effects are typically rather small for HS states.[21] Thus, using either the unrestricted HF or noninteracting KS interpretation of Θ, eq 14 simplifies readily to

$$J = \frac{E^{BS} - E^{HS}}{S^2_{max} - S^2_{min} - n^{\beta}_{nmag} + \sum_i^m \sum_j^m f_i^{\alpha,BS} f_j^{\beta,BS} |\int_{ij}^{\alpha\beta,BS}|^2} \tag{18}$$

In the special case of having only one electron on each site and considering only the magnetic orbital contribution to the overlap double sum, this expression reduces to the formula

$$J = \frac{E^{BS} - E^{HS}}{1 + |\int_{mag}^{\alpha\beta,BS}|^2} \tag{19}$$

derived earlier in ref 33 along different lines. Next, the overlap contribution of the magnetic orbitals can be simplified further for systems with more than one electron per site by treating it in two limiting cases. We will assume in the following that the α and β nonmagnetic orbitals constituting the "closed shells" are identical, i.e. $\int_{ij,nmag}^{\alpha\beta,BS} = \delta_{ij}$. The first possibility is to assume no overlap of the magnetic orbitals, i.e. "strong localization". This leads to $\Theta^{BS} = 0$ and yields

$$J = \frac{E^{BS} - E^{HS}}{S^2_{max} - S^2_{min}} \text{ if, } \int_{ij,mag}^{\alpha\beta,BS} = 0 \tag{20}$$

Furthermore, if $S_{min} = 0$ as in the case of homovalent binuclear compounds, J is given by

$$J = \frac{E^{BS} - E^{HS}}{S^2_{max}} \tag{21}$$

which is the formula obtained by Noodleman[30] a long time ago by a very different approach. The opposite approximation, i.e. "strong delocalization", consists in assuming that $\int_{ij,mag}^{\alpha\beta,BS} = 1$ when $i = j$ and zero otherwise, i.e. $\Theta^{BS} = -n^{\beta}_{mag} = -2S_B$. This treatment leads to

$$J = \frac{E^{BS} - E^{HS}}{S^2_{max} - S^2_{min} + 2S_B}, \text{ if } \int_{ij,mag}^{\alpha\beta,BS} = 1 \tag{22}$$

Using again $n^{\alpha} = n^{\beta}$, i.e. $S_{min} = 0$ and $S_{max} = 2S_B$, the exchange coupling becomes

$$J = \frac{E^{BS} - E^{HS}}{S_{max}(S_{max}+1)} \tag{23}$$

which is another formula known from the literature[55] but derived here consistently with other approximations. In addition to just rederiving known formulas for computing J in a simple and unified manner, the route taken here allows one to understand on a common basis the various approximations that are inherent to quite different approaches used previously in calculations.

2.3. Accessing the Low-Spin Total Energy. Apart from providing a way to compute J from standard electronic structure calculations, the spin-ladder idea allows one to also express the *total energy* of every spin-eigenstate in terms of the HS and BS total energies. In particular, the energy of the (antiferromagnetic) LS ground state, i.e.

$$E^{LS} = -J[\langle\hat{S}^2\rangle^{LS} - \langle\hat{S}_A^2\rangle - \langle\hat{S}_B^2\rangle] = -J[S_{min}(S_{min}+1) - S_A(S_A+1) - S_B(S_B+1)] \tag{24}$$

can be rewritten formally using the energy of the single-determinant BS state from eqs 7 and 12, i.e.

$$E^{BS} = -J[S_{min}(S_{min}+1) - S_A(S_A+1) - S_B(S_B+1)] - J[2S_B + \Theta^{BS}] \tag{25}$$

as

$$E^{LS} = E^{BS} + J[S_{max} - S_{min} + \Theta^{BS}] \tag{26}$$

Finally, by substituting the general expression for J, eq 14, a general equation for the ground-state total energy can be obtained as a sum of suitably weighted total energies of the BS and HS states

$$E^{LS} = (1+c)E^{BS} - cE^{HS} \tag{27}$$

where c is given by

$$c = \frac{S_{max} - S_{min} + \Theta^{BS}}{S_{max}^2 - S_{min}^2 - \Theta^{BS} + \Theta^{HS}} \tag{28}$$

This constitutes a convenient expression of the total energy of the low-spin, antiferromagnetically coupled ground state of a spin dimer in terms of easily accessible total energies. This general energy expression can, of course, be used in conjunction with the various approximations derived in the previous section for Θ and thus for J, which yields simplified LS total energies.

2.4. Extension of the Broken Symmetry Approach: Two-Determinant Ab Initio Molecular Dynamics. In the last section it has been shown that the total energy and thus the potential energy surface of an antiferromagnetically coupled electronic ground state may be obtained from a weighted sum of the potential energy surfaces of the HS and BS states. Consequently, forces acting on the nuclei in the antiferromagnetic LS state can be represented as a suitably weighted sum of the corresponding sets of forces

$$\mathbf{F}_I^{LS} = -\nabla_{\mathbf{R}_I}\{(1+c)E^{BS}\} - \nabla_{\mathbf{R}_I}\{-cE^{HS}\} \tag{29}$$

where it must be stressed that Θ might be a complicated function of nuclear positions and a functional of orbitals or the spin density. A dramatic simplification is achieved by invoking the above-mentioned approximation of no overlap of the magnetic orbitals and no spin contamination according to eq 20 (or eq 21 for the $n^\alpha = n^\beta$ special case). This implies that

$$c \approx \frac{S_{max} - S_{min}}{S_{max}^2 - S_{min}^2} \tag{30}$$

so that $\mathbf{F}_I^{LS}$ is obtained as a linear combination from

$$\mathbf{F}_I^{LS} = (1+c)\mathbf{F}_I^{BS} - c\mathbf{F}_I^{HS} \tag{31}$$

since c is just a constant parameter in this limit. Effects due to spin contamination and overlap of magnetic orbitals will be discussed later in the manuscript.

At this stage, one can formulate AIMD very efficiently in the framework of a Car−Parrinello Lagrangian[56,57] generalized to two determinants

$$\begin{aligned} L_{CP}^{LS} = {} & \frac{1}{2}\sum_I^N M_I\dot{\mathbf{R}}_I^2 \\ & + \frac{1}{2}\sum_i \{(1+c)[\mu\langle\dot{\varphi}_i^{BS}|\dot{\varphi}_i^{BS}\rangle] \\ & - c[\mu\langle\dot{\varphi}_i^{HS}|\dot{\varphi}_i^{HS}\rangle]\} \\ & - \{(1+c)E^{BS}[\{\varphi_i^{BS}\},\{\mathbf{R}_I\}] \\ & - cE^{HS}[\{\varphi_i^{HS}\},\{\mathbf{R}_I\}]\} \\ & + \sum_{i,j}\{(1+c)[\Lambda_{ij}^{BS}(\langle\varphi_i^{BS}|\varphi_j^{BS}\rangle - \delta_{ij})] \\ & - c[\Lambda_{ij}^{HS}(\langle\varphi_i^{HS}|\varphi_j^{HS}\rangle - \delta_{ij})] \end{aligned} \tag{32}$$

by expressing all the contributions to the Lagrangian depending on the electronic structure as a linear combination of the BS and the HS states. Note that two independent sets of KS orbitals, $\{\varphi_i^{HS}\}$ and $\{\varphi_i^{BS}\}$, are used to built up the KS determinants underlying the HS and BS total energy expressions. Correspondingly, the equations of motion for N nuclei with mass $\{M_I\}$ are given by

$$M_I\ddot{\mathbf{R}}_I = -(1+c)(\nabla_{\mathbf{R}_I}E^{BS}) + c(\nabla_{\mathbf{R}_I}E^{HS}) \tag{33}$$

whereas the orbitals move according to

$$\begin{aligned} \mu\ddot{\varphi}_i^{BS} &= -(1+c)(\nabla_{\varphi_i^{BS}}E^{BS} + f_{constr}^{BS}) \\ \mu\ddot{\varphi}_i^{HS} &= c(\nabla_{\varphi_i^{HS}}E^{HS} + f_{constr}^{HS}) \end{aligned} \tag{34}$$

Here, μ is the ficticious mass of the orbitals, and f_{constr} are the forces due to the orthonormality constraints imposed on the orbitals. These equations show that within this approach the BS and the HS wave functions are simultaneously propagated under the constraint that the orthonormality condition, imposed by the Lagrange multipliers $\{\Lambda_{ij}\}$, is satisfied by the two sets of orbitals individually. Thus, the nuclear dynamics is performed on the ground-state LS energy hypersurface obtained by a projection according to eq 27. Note that if thermostats for the electronic wave functions are invoked,[57] the thermostat energy must be calculated according to the projection scheme as well.

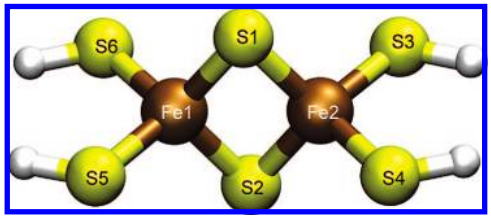

Figure 2. Minimum model system for binuclear iron−sulfur complexes with atomic labeling. Color scheme: iron atoms are brown, sulfur atoms are yellow, and hydrogen atoms are gray.

We will be referring to the above introduced approach as extended broken-symmetry (EBS) scheme. Most importantly, this EBS approach allows one to perform molecular dynamics in the antiferromagnetically coupled ground state of a binuclear complex. Of course, this method can be used immediately to optimize the structure of such complexes or to perform vibrational analysis in the harmonic approximation. Finally, when it comes to computing J it is worth noting that only such an approach is intrinsically consistent where the same approximate spin-projection scheme is used to optimize first the structure for which J is then obtained at no additional cost. It is noted in passing that the afore derived EBS scheme can be directly implemented in the framework of wave function-based or density functional-based methods.

2.5. Computational Setup. In the minimum model used here for [2Fe-2S] complexes, i.e. $[Fe_2S_2(SH)_4]^{2-}$ in isolation, the Fe_2S_2 core is capped by four SH^- groups according to Figure 2, which mimic cysteinyl ligands as found in typical protein environments.[10] This model complex has been studied first using Xα valence bond theory[58] and later using semiempirical as well as configuration interaction (CI) techniques.[59] The EBS method has been implemented into the CPMD simulation package[57,60] which was used for structure optimization as well as for AIMD simulations all performed within the spin-unrestricted Kohn−Sham density functional theory in its plane wave/pseudopotential formulation.

The PBE[61,62] exchange-correlation functional was chosen, and the core electrons were taken into account using Vanderbilt's ultrasoft pseudopotentials[63] which contain additional d-projectors in the case of sulfur as well as scalar relativistic corrections and semicore states for iron; note that other functionals of the generalized gradient approximation type could be used here instead. For the ultrasoft pseudopotentials a rather low plane wave cutoff of 30 Ry was sufficient to obtain convergence in the forces of the nuclei. The simulation cell was an unusually large cubic box with a constant edge length of 16.9 Å which turned out to be necessary in order to converge the representation of the density for such a 2-fold negatively charged complex. The charge of the system was decoupled from its periodic images using the Martyna-Tuckerman Poisson solver to impose cluster boundary conditions.[64]

The structure optimizations were performed for the single-determinant HS and BS states as well as for the projected LS state within the two-determinant EBS scheme. If not otherwise stated the approximations to eq 18 leading to eq 21 to compute J[30] and eq 27 together with eq 30 to calculate E^{LS} were used throughout this paper. The criteria were 10^{-4} and 10^{-7} a.u. for the forces on ions and the gradient of the wave function, respectively. The AIMD simulations were performed using Car−Parrinello propagation[56] along with separate Nosé-Hoover chain[65] thermostats for nuclei and electronic orbitals. The system was thermostatted at 300 K, and a time step of 0.145 fs was used for the integration of the equations of motion. The fictitious mass for the orbitals was 700 a.u., and the hydrogen (H) mass was substituted by the deuterium (D) mass in all dynamical calculations. The minimum energy structures from the structure optimization were taken as initial configurations and equilibrated for approximately 5 ps at 300 K thermostatting every degree of freedom individually ("massive thermostating") to ensure energy equipartition between all vibrational modes. Subsequently, 17 ps long trajectories were collected using one thermostat for the complete system.

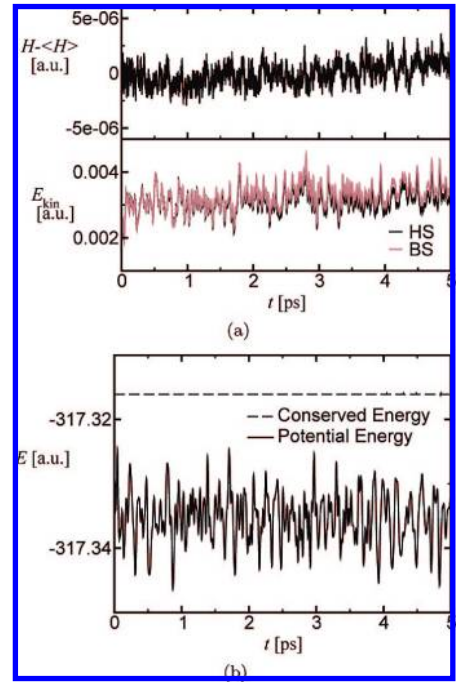

Figure 3. Energy conservation during a microcanonical AIMD simulation in the two-determinant EBS formalism. (a) Upper panel: instantaneous deviation of the conserved energy H from its average value, $H-\langle H\rangle$; lower panel: fictitious kinetic energy of the orbitals, E_{kin}, for the BS (brown) and HS (black) determinants. (b) Conserved energy (dashed line) on the scale of the EBS potential energy (solid line). All energies are reported in a.u.

3. Results and Discussion

3.1. Stability of EBS–CP Molecular Dynamics. To assess the stability of the two-determinant Car−Parrinello propagation, different energies were calculated from microcanonical EBS simulations of the minimum model $[Fe_2S_2(SH)_4]^{2-}$ for iron−sulfur complexes as shown in Figure 3. At variance with the simulation parameters described in section 2.5 and used later for the analysis of the magneto-structural dynamics of the complex, no thermostats were employed, hydrogen atoms were used instead of deuterium, and the integration time step was therefore 4 au (≈0.1 fs) in

Table 1. Structural Data for the Iron−Sulfur Complex in Different Spin States[a]

distance [Å]	HS	BS	EBS
Fe1−Fe2	2.960	2.676	2.622
S1−S2	3.488	3.488	3.467
Fe1−S1	2.284	2.197	2.172
Fe1−S2	2.297	2.194	2.170
Fe2−S1	2.290	2.202	2.177
Fe2−S2	2.279	2.198	2.176
angle [°]	**HS**	**BS**	**EBS**
S2−Fe1−S1	99.1	105.2	107.0
S2−Fe2−S1	99.5	104.9	105.6
Fe1−S1−Fe2	80.6	74.9	74.2
Fe1−S2−Fe2	80.6	75.1	74.2
rmsd (Fe_2S_2) [Å]	0.123	0.020	0.0
rmsd ($Fe_2S_2S_4$) [Å]	0.174	0.020	0.0
J [cm^{-1}]	−227	−390	−435

[a] Selected structural properties and the coupling constant J of $[Fe_2S_2(SH)_4]^{2-}$ in vacuo in the high-spin (HS), broken-symmetry (BS), and extended broken-symmetry (EBS) states resulting from structure optimization in the corresponding state. J is computed using eq 21 in all cases.

this case. All other parameters were identical to those described in section 2.5.

In Figure 3(a) the deviation from the average of the conserved energy,[57] H-$\langle H\rangle$, is plotted along with the ficticious kinetic energy of the electrons, E_{kin}, for both BS and HS determinants. On the simulated time scale of 5 ps the fluctuations are within 4.0×10^{-6} a.u., and there is no appreciable drift in conserved energy. This is affirmed by Figure 3(b), which shows the conserved and the potential energies on the same scale. Also the ficticious kinetic energy of the orbitals had no drastic shifts or oscillations and behaved well during the entire simulation (see the lower panel in Figure 3(a)).

3.2. Structure Optimization. The first point to be addressed is the impact of the two-determinant total energy scheme on the structure of the $[Fe_2S_2(SH)_4]^{2-}$ complex in vacuo, i.e. a comparison between structures optimized using the EBS scheme with eqs 30 and 31, compared with the structures optimized using the conventional single-determinant unrestricted BS and HS states. At the same time we determine the effect of these structural changes on the coupling constant J which is evaluated within the approximation eq 21 in all the three cases. Usually in literature, J is computed by optimizing the structure within the unrestricted BS approach, i.e. using E^{BS} only.

Concerning essential structural features such as iron−iron distance or iron−sulfur−iron angle the BS and the EBS optimized structures are found to be quite similar, whereas the complex is more open in the HS state, see Table 1. This is confirmed by the root-mean-square-deviations (rmsd) of the atomic positions relative to the EBS structure as compiled in Table 1.

The rmsd values of the bare core are 0.020 Å and 0.123 Å for the broken-symmetry and the high-spin state, respectively. If the ligand sulfur atoms S3-S6 are taken into account additionally, the rmsd value for the high-spin case increases to 0.174 Å, but the trend remains the same. Closer inspection of the data in Table 1 indicates that the main differences in the structure are due to the changes in bond lengths and angles in the Fe_2S_2 core, whereas the other bond lengths and angles are very similar. In a previous study[66] single point LS energies have been computed employing Noodleman's approach, i.e. eqs 27 and 30, at various Fe−Fe distances for a similar system, $[(Fe_2S_2)(SCH_3)_4]^{2-}$. The conclusion that the Fe−Fe distance becomes shorter upon going from the BS state to the spin-projected LS structure is in agreement with our observation.

3.3. Exchange Coupling Constant. More pronounced is the effect of the structural changes due to spin-projection on the value of the exchange coupling constant J when obtained consistently at the respective optimized structures. Clearly, the EBS structure is most compact and thus yields the largest, i.e. most negative, antiferromagnetic coupling constant, whereas $|J|$ is smallest for the least compact HS structure. Overall, the J value can change by nearly a factor of 2 depending on the structure used to compute it.

To our knowledge no converged quantum chemical J values are available even for this simple system. But for related systems[67] the absolute value of the coupling constant is smaller by a factor of 2−3 in experiment as compared to the present calculations. However, such an overestimation of $|J|$ is a well-known artifact of using the local density approximation (LDA), or functionals of the generalized gradient approximation (GGA) type,[68–70] and may be attributed to the self-interaction error (SIE), whereas using only Fock exchange underestimates J considerably, see the lucid discussion in ref 25. In standard KS density functional calculations using LDA or GGA functionals the SIE tends to delocalize the magnetic orbitals, leading to a stronger bonding and thus to shorter bond distances. In particular, such an error can result in an overestimation of the overlap of magnetic orbitals and thus of $|J|$.

The problem can be reduced using self-interaction correction (SIC) schemes,[71] for instance in simplified versions,[72–75] or DFT+U methods.[76–80] There are also recent efforts to improve the calculation of J values by exploiting the virtues of constrained DFT techniques[81] in the framework of magnetic complexes.[82,83] As an alternative approach it was demonstrated that accurate J values can also be obtained by the tuning the Fock exchange contribution in hybrid functionals such as B3LYP[84] at the expense of adjusting density functionals for computing a particular property. It is mentioned in passing that these and similar schemes can be combined with our EBS approach thus improving the approximate DFT description of the BS state as such.

A recent study advocates that formula eq 23 should yield very good results for the exchange coupling constant compared to experiment *if no SIC is applied*.[70] This idea can be analyzed within the present framework; see also ref 25 for a discussion of this proposal. In deriving eq 23 from eq 18 within the general framework laid out in section 2.2 the approximation of assuming full overlap of magnetic orbitals, i.e. strong delocalization, was imposed to evaluate the spin contamination in the BS state only, whereas strong localization and thus no overlap was assumed in the HS state as usual. Obviously this increases the denominator by the

Table 2. Structural Data for in Vacuo Optimized $[Fe_2S_2(SH)_4]^{2-}$ Complex Using Different Values for the Overlap of Magnetic Orbitals[a]

Θ^{BS}	0.000	−0.313	−1.250	−2.813	−5.000
$\int^{\alpha\beta,BS}_{ii,mag}$	0.00	0.25	0.50	0.75	1.00
c	0.200	0.185	0.143	0.079	0.000
distance [Å]					
Fe1−Fe2	2.622	2.626	2.637	2.655	2.676
S1−S2	3.467	3.470	3.475	3.481	3.488
Fe1−S1	2.172	2.174	2.179	2.188	2.197
Fe1−S2	2.170	2.172	2.177	2.185	2.194
Fe2−S1	2.177	2.178	2.183	2.193	2.202
Fe2−S2	2.176	2.180	2.185	2.190	2.198
angle [°]					
S2−Fe1−S1	107.0	106.0	105.8	105.5	105.2
S2−Fe2−S1	105.6	105.6	105.4	105.2	104.9
Fe1−S1−Fe2	74.2	74.2	74.4	74.6	74.9
Fe1−S2−Fe2	74.2	74.3	74.4	74.7	75.1
J [cm^{-1}]	−435	−426	−402	−366	−325

[a] Selected structural properties and coupling constant J of $[Fe_2S_2(SH)_4]^{2-}$ in vacuo using different values for the spin correction term Θ^{BS} while keeping $\Theta^{HS} = 0$. The corresponding values of overlap of magnetic orbitals $\int^{\alpha\beta,BS}_{ii,mag}$ when $\int^{\alpha\beta,BS}_{ij,mag} = 0.0$ for $i \neq j$. Note that $\Theta^{BS} = -5.0$ results in a structure identical to the BS structure (see Table 1); however, the J values are different as they were computed using eq 18 with different values of Θ^{BS}; see text for details.

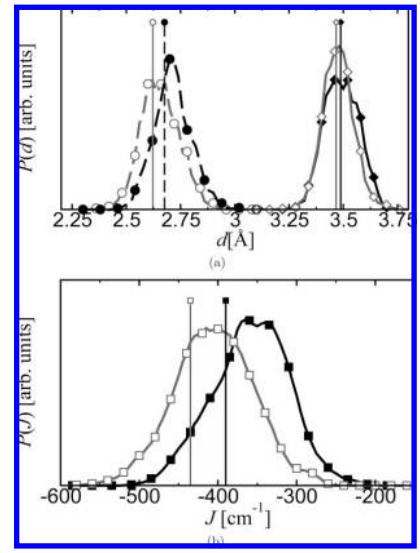

Figure 4. Probability distribution functions for selected structural quantities and J of the $[Fe_2S_2(SH)_4]^{2-}$ complex for BS and EBS-AIMD. Normalized probability distribution functions of (a) the Fe1−Fe2 (broken line, circles) and S1−S2 (solid line, diamonds) distance and (b) of the coupling constant J (solid line, squares) obtained from AIMD of the $[Fe_2S_2(SH)_4]^{2-}$ complex at 300 K in vacuo using the BS (black, filled symbols) and EBS (gray, open symbols) schemes. The corresponding values obtained for the optimized minimum energy structures are shown as vertical bars using the same labeling.

term $+S_{max}$ compared to eq 21 and thus decreases the value of $|J|$ accordingly. The assumption of full overlap results in $\Theta^{BS} = -n^{\beta}_{mag} = -S_{max}$ and $S_{min} = 0$ having $n^{\alpha} = n^{\beta}$. From eq 28 follows, $E^{LS} = E^{BS}$ as $c = 0$ in eq 27. Thus, the true multideterminantal LS ground state is effectively approximated by the single-determinant BS state. Besides, this approximation is intrinsically inconsistent because full overlap of the magnetic orbitals implies a closed shell electronic configuration, but an unrestricted BS determinant is used instead.

At this point it is worth estimating the effect of the spin correction term Θ^{BS} which includes the degree of overlap of magnetic orbitals on both structure and coupling constant J. These properties are easily accessible within the EBS approach on equal footing. In order to work out these trends qualitatively, we change the value of Θ from its maximum value of 0 to its minimum value of −5.0. The structure of the complex was independently optimized for each value of Θ^{BS} using the forces eq 29 with c according to eq 28 and J is computed using eq 14 correspondingly. For the sake of simplicity this can be viewed as a systematic change in the overlap of the magnetic orbitals $\int^{\alpha\beta,BS}_{ii,mag}$, assuming $\int^{\alpha\beta,BS}_{ij,mag} = 0$ for $i \neq j$; note that as usual Θ^{HS} was always kept zero.

The data compiled in Table 2 show that distances are more affected than angles. It is important to note here that the structure optimized using $\Theta^{BS} = -5.0$ (see Table 2) within the EBS scheme results in a structure which is identical to that optimized just using the BS state (see Table 1). But the J values of 325 and 390 cm^{-1} for this structure were obtained using eq 18 with $\Theta^{BS} = -5.0$ (in Table 2) and using eq 21 (in Table 1), respectively. It is apparent from this comparison that the larger the overlap term $\int^{\alpha\beta}$ the more open is the resulting structure and thereby the smaller the magnitude of J. Thus, the structure as well as the value of the coupling constant could be easily "tuned" by changing the overlap term, as effectively done in ref 70. However, the assumption of full overlap of magnetic orbitals seems less justified in the case of weakly coupled dimers than the other limiting case, which is the assumption of zero overlap.[25] Furthermore, imposing extreme delocalization is inconsistent with the basic assumption underlying the validity of the Heisenberg model in eq 1, which is the basis of the present and related spin-projection schemes.

3.4. Dynamical Effects on Structure and *J*. In order to relate the dynamics of the antiferromagnetic coupling constant J to the structural dynamics of the iron−sulfur complex within the BS and the EBS schemes, Car−Parrinello AIMD simulations were performed using both approaches. The same trend as obtained by structure optimizations is seen in both the average structural quantities and the J values sampled from molecular dynamics trajectories (see Figure 4(a) and Figure 4(b), respectively).

The average values of J are −356 and −403 cm^{-1} for the BS and EBS case, respectively, which is a 10−15% effect on the coupling constant when considering the two-determinant EBS structure consistent with the spin-projection formula used to compute J, instead of simply using the single-determinant BS structure. In addition, the rather broad probability distributions of J clearly demonstrate J is fluctuating with considerable amplitudes at 300 K covering the range from −600 to −300 cm^{-1} in case of the EBS approach. These results underline the need of considering dynamical behavior of such a spin-coupled complex when

studying its magnetic properties, since J can change by a factor of 2 just because of thermal fluctuations at room temperature!

The corresponding averages of the Fe−Fe and the S−S distances within the core are different for the conventional and the extended broken-symmetry schemes, indicating different minima on the free energy surface (FES) even at room temperature. Additionally, since the widths and thus the fluctuations are also different, the shapes of the underlying FES in the sampled regions differ as well. While the average distances of the two bridging sulfur atoms are almost the same as in the minimum energy structures (cf. the vertical bars), the Fe−Fe distances are shifted to larger values in both schemes compared to the respective optimized structures. Together with the fact that the most probable distances (determined by the minimum of the PES) and the average distances (determined by the minimum of the FES) are not equal, this implies that the observed effect is due to an asymmetric anharmonicity in the effective Fe−Fe interactions.

3.5. Dynamical Structural Properties. The different FES produced by the two methods should be mirrored in the *dynamical behavior* of this iron−sulfur complex as well. To investigate the dynamical behavior of a property **P**, it is appropriate to define a correlation function

$$G_{\mathbf{PP}}(t) = \frac{\langle \mathbf{P}(t_0)\cdot\mathbf{P}(t_0+t)\rangle_{t_0}}{\langle \mathbf{P}(t_0)\cdot\mathbf{P}(t_0)\rangle_{t_0}} \tag{35}$$

where $\langle ... \rangle_{t_0}$ implies the usual average over the reference time points t_0 along the generated trajectory. Its Fourier transform

$$G_{\mathbf{PP}}(\omega) = \frac{1}{2\pi}\int_{-\infty}^{\infty} G_{\mathbf{PP}}(t)\exp(-i\omega t)dt \tag{36}$$

represents the spectral density, or the power spectrum, of the corresponding property and can be used to define an "absorption coefficient"

$$A_{\mathbf{PP}}(\omega) = \omega^2 G_{\mathbf{PP}}(\omega) \tag{37}$$

which already includes the so-called harmonic quantum correction factor.[85]

To explore the structural dynamics of the complex, it is convenient to use the (nuclear) velocity autocorrelation function, $G_{\dot{\mathbf{R}}\dot{\mathbf{R}}}(t)$ where $\dot{\mathbf{R}}$ is a vector that contains the velocities of all or selected nuclei in the complex. The resulting spectra obtained from the EBS and the BS trajectories at 300 K in vacuo are shown in Figure 5.

At first glance they appear similar, and in both cases two distinct spectral regions can be identified. The high frequency region around 1750 cm^{-1} is assigned to S-D vibrations, whereas the region below about 500 cm^{-1} is comprised of iron−sulfur motion; recall that H was substituted by D for technical reasons. But on a closer look the spectra obtained by autocorrelating only the four atoms in the Fe_2S_2 core in Figure 5(b) are seen to display differences. In particular the EBS spectrum is broader at the high-frequency wings and more structured in the region between about 200 and 400 cm^{-1}.

The individual features of these spectra can only be understood after performing a spectral decomposition. To achieve this it is necessary to choose a basis in which the

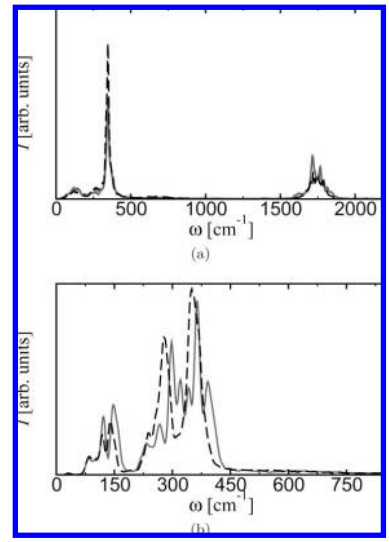

Figure 5. Spectra $A_{\dot{\mathbf{R}}\dot{\mathbf{R}}}(\omega)$ of the velocity autocorrelation function obtained according to eq 37 from AIMD simulations of the $[Fe_2S_2(SH)_4]^{2-}$ complex in vacuo for (a) the full system and (b) only the four atoms in the Fe_2S_2 core using the BS (dashed lines) and EBS (solid lines) methods.

dynamics can be expressed. Since the atoms of the Fe_2S_2 core are expected to affect the magnetic properties much more than the four peripheral SH^- groups, we will restrict the investigation to the dynamics of the Fe_2S_2 core in terms of normal modes of the Fe_2S_2 fragment. However, it is clear that the ligands also affect the internal motion of the core due to coupling effects.

Taking into account the approximate D_{2h} symmetry of the average structure of the Fe_2S_2 core from the AIMD simulation, it is appropriate to use corresponding symmetry-adapted normal modes as a basis. There exist six modes, $\{\mathbf{q}_\xi\}$ (see Figure 6), apart from rigid rotations and translations. Generally, a coupling of the modes is expected during a molecular dynamics trajectory. But by taking an appropriate linear combination of these modes, it is possible to generate a set of new modes, $\{\tilde{\mathbf{q}}_\xi\}$, with minimal coupling. The coefficients for the linear combination were obtained by minimizing $\int|A_{\xi,\xi'}(\omega)|d\omega$. The spectrum $A_{\xi,\xi'}(\omega)$ is calculated according to eqs 36 and 37 from the corresponding cross-correlation function

$$G_{\xi,\xi'}(t) = \frac{\langle q_\xi(t_0)q_{\xi'}(t_0+t)\rangle_{t_0}}{\langle q_\xi(t_0)q_{\xi'}(t_0)\rangle_{t_0}}; \xi \neq \xi', \xi = 1, \ldots, 6 \tag{38}$$

Here, $\{q_\xi(t)\}$ denote the projections of the mass-weighted nuclear positions of the Fe_2S_2 core, $\mathbf{R}_c(t)$, along the molecular dynamics trajectory on each of the six basis functions $\{\mathbf{q}_\xi\}$

$$q_\xi(t) = \mathbf{R}_c(t)\cdot\mathbf{q}_\xi \tag{39}$$

normalized to zero mean and unit variance where $\mathbf{R}_c(t)$ are in the frame of reference given by the basis.

The modes $\{\tilde{\mathbf{q}}_\xi\}$ obtained by this procedure were used to calculate the spectra $A_{\xi\xi}(\omega)$ according to eqs 36 and 37 from the corresponding autocorrelation functions $G_{\xi\xi}(t)$. In Figure 7 the individual spectral components $A_{\xi\xi}(\omega)$ are shown

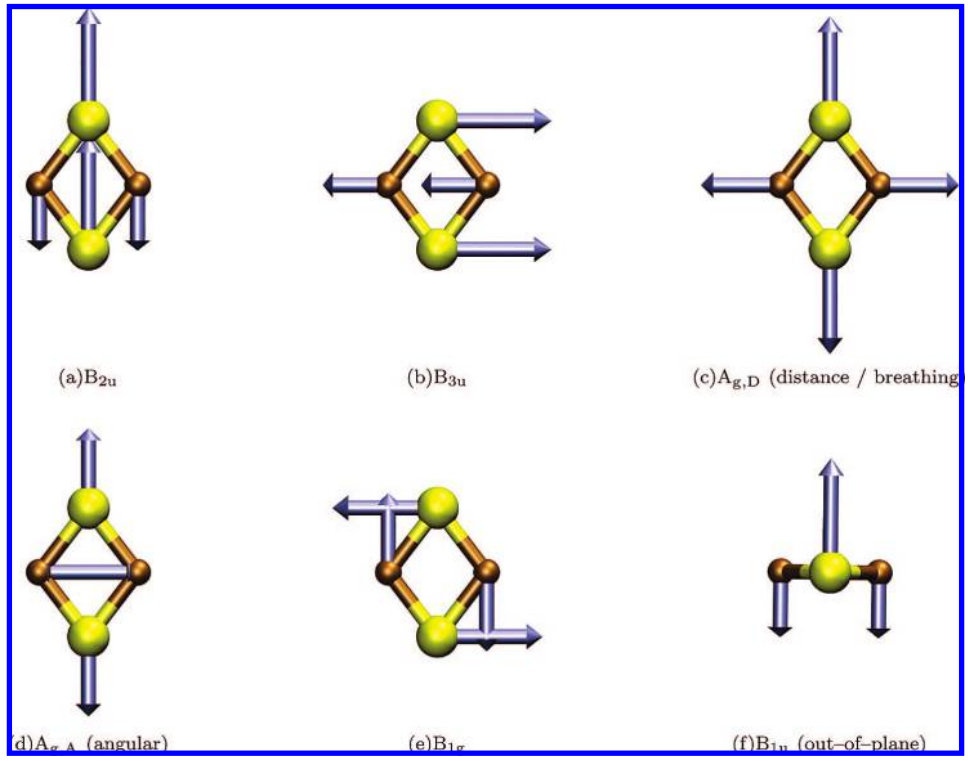

Figure 6. Ideal D_{2h} symmetry-adapted normal modes, $\{\mathbf{q}_\xi\}$, for the Fe_2S_2 core of the $[Fe_2S_2(SH)_4]^{2-}$ complex. The small brown and large yellow spheres represent iron and sulfur atoms, respectively. The blue arrows show the phases and relative magnitudes of the atomic displacements along each mode.

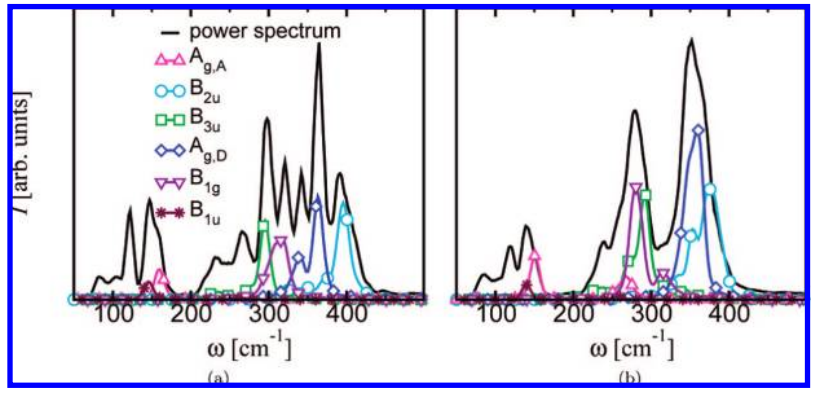

Figure 7. Spectral decomposition of the spectra $A_{\dot{R}\dot{R}}(\omega)$ of the Fe_2S_2 core obtained from AIMD of the $[Fe_2S_2(SH)_4]^{2-}$complex in vacuo using (a) the EBS and (b) the BS approaches. The spectral components, $A_{\xi\xi}(\omega)$, were smoothened by a convolution with a Gaussian function of 5 cm^{-1} width.

together with the full spectrum obtained for the Fe_2S_2 fragment. In the following, the modes $\tilde{\mathbf{q}}_\xi$ are referred to according to their largest $\mathbf{q}_\xi$ component which always exceeds 97%. Due to the loss of structural symmetry during the dynamics, *g* and *u* modes can couple to each other. Note, since a normalization to zero mean and unit variance was performed for the individual $\tilde{q}_\xi$, the relative intensities are preserved only within the individual spectra $A_{\xi\xi}(\omega)$.

First, the EBS vibrational spectrum is analyzed along these lines. Its spectral decomposition in Figure 7(a) shows that the out-of-plane vibration B_{1u} leads to a resonance at 145 cm^{-1}. The B_{3u} and the B_{1g} in-plane vibrations appear at 295 cm^{-1} and 318 cm^{-1}, respectively. The former shows an additional peak at 235 cm^{-1}. The B_{2u} mode spans a rather broad spectral range (300−430 cm^{-1}) having a sharp peak at 396 cm^{-1} in addition to a weak intensity region at 300−375 cm^{-1}. The latter could be attributed to a slight coupling to the $A_{g,D}$ vibration. The $A_{g,A}$ angular mode gives rise to a peak at 160 cm^{-1}, where a slight mixing with B_{1u} occurs. Also in the spectrum of the $A_{g,D}$ vibration two signals are observable, at 340 cm^{-1} and 364 cm^{-1}. Despite the decorrelation procedure, residual mixing of this motion with several other modes (B_{2u}, B_{3u}, B_{1g}, and $A_{g,A}$) could not be avoided, which is, however, weak.

In the BS scheme the spectrum is less complex (see Figure 7(b)) as that of EBS. All modes exhibit a red shift of their frequencies with respect to the EBS spectrum. The strongest shifts are observed for the B_{1g} and the B_{2u} vibrations, which are 35 and 20 cm^{-1}, respectively. Other modes are only slightly shifted (up to 5 cm^{-1}). Another striking difference

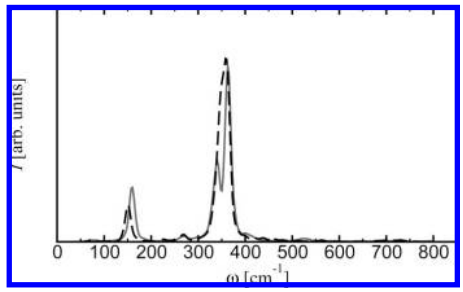

Figure 8. Spectra $A_{JJ}(\omega)$, calculated from the autocorrelation function of $J(t)$ from AIMD of the $[Fe_2S_2(SH)_4]^{2-}$ complex in vacuo using the BS (black dashed line) and EBS approaches (gray solid line).

is that the $A_{g,D}$ breathing mode exhibits a double peak in the EBS case (340 and 364 cm^{-1}) but has only a single peak (360 cm^{-1}) with a shoulder (350 cm^{-1}) in the BS scheme. It turns out that the mixing of the two A_g modes is slightly weaker compared to the EBS situation. Interestingly, the B_{2u} mode couples very strongly to the $A_{g,D}$ vibration in the BS case. This coupling could not be removed by the decorrelation procedure described above.

We note in passing that the remaining mixing of the individual vibrational modes is attributed to a deviation from the harmonic picture or to the interactions of the corresponding modes via the four SH^- ligands as noted in the beginning of this section. Indeed, principal component analysis[86] (PCA) of the trajectories shows, for example, modes in which the core motion shows $A_{g,A}$ character combined with symmetric and asymmetric ligand vibrations (data are not shown here but see ref 87 for full analysis). Ligand contributions are also responsible for the features up to 125 cm^{-1} and the peaks at 267 and 240 cm^{-1} in Figures 7(a) and 7(b), respectively, which are not fully explained by $\{\tilde{\mathbf{q}}_\xi\}$. Also in this case PCA could reveal modes which show signals in these particular regions.[87]

3.6. Dynamical Magnetostructural Properties. In a simple orbital picture the value of the exchange coupling constant J is related to the interactions among singly occupied orbitals, which are mainly located in the Fe_2S_2 core. Thus, changes of the structure due to the dynamical evolution of the four core atoms are expected to most directly affect J and, thereby, imprint a time-dependence, $J(t)$. This time-dependent exchange coupling $J(t)$ is most conveniently analyzed in Fourier space, i.e. in terms of its spectrum $A_{JJ}(\omega)$ calculated according to eqs 36 and 37 from the autocorrelation function $G_{JJ}(t)$ defined in eq 35.

The power spectra resulting from the two-determinant EBS and one-determinant BS dynamics depicted in Figure 8 feature two main resonances at about 150 and 350 cm^{-1} and an additional, small feature around 270 cm^{-1}. Moreover, the lower frequency peak at $\approx$150 cm^{-1} is slightly red-shifted in the BS case w.r.t. the EBS reference where the 350 cm^{-1} resonance is clearly split in addition.

To reveal the relationships between the structural dynamics of the complex unraveled in section 3.5 and the "magneto-dynamics" embodied in $A_{JJ}(\omega)$, it is appropriate to analyze the frequency dependent correlations of $J(t)$ with the individual contributions of the different vibrational motion, $\tilde{q}_\xi(t)$

$$G_{J\xi}(t) = \frac{\langle \tilde{J}(t_0)\tilde{q}_\xi(t_0+t)\rangle_{t_0}}{\langle \tilde{J}(t_0)\tilde{q}_\xi(t_0)\rangle_{t_0}} \tag{40}$$

where $\tilde{J}$ indicates a zero mean and unity variance normalization of $J(t)$. The spectra calculated from these cross-correlation functions using eqs 36 and 37, $A_{J\xi}(\omega)$, clearly display frequency dependent correlations of magnetic and structural dynamics.

The spectrum of the exchange coupling constant, $A_{JJ}(\omega)$, and the spectral components of the individual vibrational modes, $A_{\xi\xi}$, are shown for the EBS and BS results in Figures 9(a) and 9(c), respectively. In both cases several vibrational modes can be identified in those frequency regions where $J(\omega)$ has large intensity. However, the more sophisticated cross-correlation spectra (see Figures 9(b) and 9(d)) clearly show that all features of $A_{JJ}(\omega)$ for both the EBS and the BS results can be explained using mainly the two A_g modes.

In particular, the peak at 160 cm^{-1} and the small feature at 267 cm^{-1} in $A_{JJ}(\omega)$ of the EBS simulation are both due to $A_{g,A}$ vibrations, while the $A_{g,D}$ symmetric motion is related to the peaks at 340 and 364 cm^{-1}. Other modes show relatively small intensities in the cross-correlation spectra thus indicating only minor contributions to the magneto-structural dynamics of J.

The influence of the individual modes on the coupling constant can be understood qualitatively by recalling the nature of the superexchange interaction,[23] in particular how the vibrations of the core atoms influence the exchange pathways from one iron atom to the other via the sulfur bridges. It is clear that increasing Fe−S distances as well as decreasing Fe−S−Fe angles will decrease the superexchange. Along the two A_g modes, see Figure 6(c),(d), both superexchange paths are always affected in a symmetric manner. For the $A_{g,D}$ mode both paths simultaneously become shorter or longer thus enhancing or weakening the superexchange interaction; note that the Fe−S−Fe angles remain constant along displacements according to this symmetry. On the other hand, along the $A_{g,A}$ motion the weakening and enhancing of the superexchange is affected by a symmetric increase and decrease in the Fe−S−Fe angles, respectively.

In the BS case the overall picture is similar; the two A_g modes contribute most to the dynamics of the exchange coupling. However, Figure 9(d) shows an additional cross-correlation of $J(t)$ with the B_{2u} vibrational component. This mode couples very strongly to the $A_{g,D}$ vibration. This coupling could not be removed by the decorrelation procedure described in the previous section (data not shown) indicating a deviation from the imposed harmonic picture or a coupling via ligand modes. Moreover, PCA results show that, unlike in the EBS case, the B_{2u} mode of the BS simulations deviates more strongly from the perfect symmetry (see ref 87 for full analysis). This deviation might be responsible for the mutual coupling of $A_{g,D}$ and B_{2u}, directly

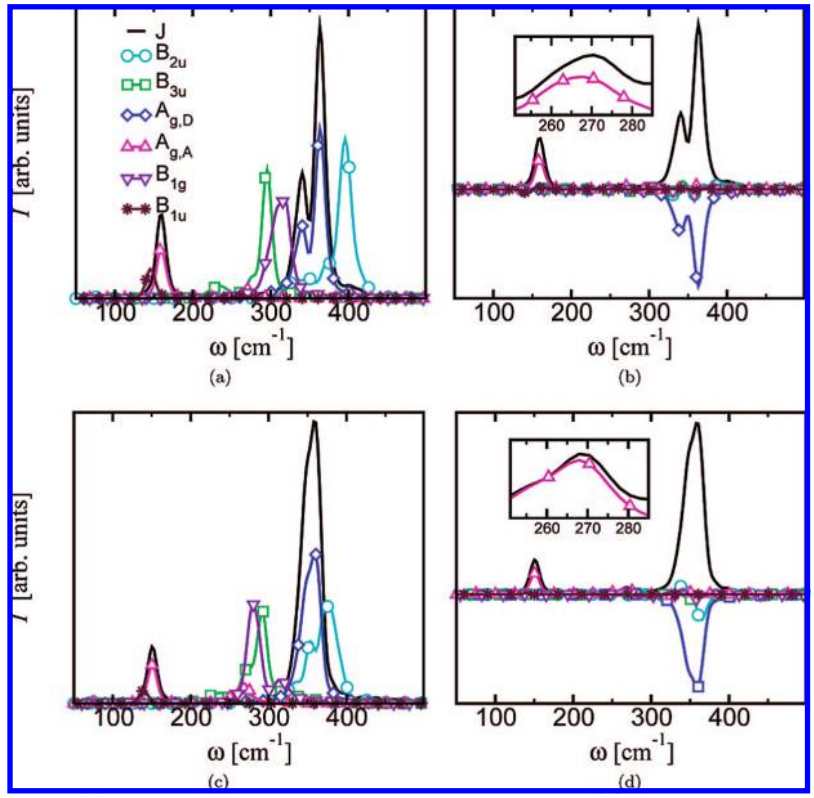

Figure 9. Spectra $A_{JJ}(\omega)$, together with the vibrational spectral components, $A_{\xi\xi}(\omega)$, of the Fe_2S_2 core dynamics obtained from AIMD of the $[Fe_2S_2(SH)_4]^{2-}$ complex in vacuo using (a) the EBS and (c) the BS approaches. Panels (b) and (d) show the corresponding frequency dependent cross correlations, $A_{J\xi}(\omega)$, between $J(t)$ and the individual vibrational components, $\tilde{q}_\xi(t)$, together with $A_{JJ}(\omega)$ for the EBS and BS approaches, respectively.

or via ligand vibrations, and causes an incomplete cancelation of the positive and negative contributions to the exchange interaction.

Overall, the BS and EBS schemes provide a qualitatively similar picture of the influence of the skeleton vibrations on the dynamics of the magnetic coupling constant J, i.e. on the dynamical magnetostructural properties of this iron−sulfur complex. In both approaches $A_{JJ}(\omega)$ shows a high and a low frequency domain, which can be ascribed to the $A_{g,D}$ and $A_{g,A}$ modes, respectively. Reinforcing the previous finding observed from the optimized structures, the exchange coupling J differs depending on the used scheme alike the average structures. Within the EBS scheme a more compact average structure is obtained, and thus the average $|J|$ value is about 10−15% larger (403 vs 356 cm^{-1}) in the two-determinant EBS approach compared to the one-determinant BS approximation. Moreover, apart from a slight blue shift of the EBS vibrations and thus the resonances in $A_{JJ}(\omega)$ with respect to their BS counterparts, the mixing of modes and their interplay with the ligands differ. In particular, coupling of the B_{2u} and $A_{g,D}$ modes is observed in the BS case. One manifestation of this different coupling pattern is the pronounced double peak feature at 340 and 364 cm^{-1} in the EBS case which appears as a single peak in the BS spectrum (at 360 cm^{-1} with a very weak shoulder at 350 cm^{-1}).

Conventionally, the magnetic exchange coupling in bridged binuclear transition metal complexes is discussed by means of the Goodenough-Kanamori rules[38–40] which relate the sign and the size of the coupling constant J to the symmetry of the magnetic orbitals, the coordination of the metal cations, and the structure of the diamagnetic bridge. In the present treatment we are able to go far beyond this static picture and correlate the structural changes of the Fe_2S_2 core with the fluctuations of the antiferromagnetic coupling at finite temperature. This opens the doorway to a direct comparison between calculated and measured magnetic properties of metalloproteins. It should also be mentioned that the Good-enough-Kanamori rules[38–40] give no prediction for the exchange coupling of two d^5 metal cations in tetrahedral coordination.

4. Summary, Conclusions, and Outlook

In order to understand the structural, but in particular the dynamical, properties of antiferromagnetically coupled bi-nuclear transition metal complexes, a novel *dynamical* method is introduced. This density functional based scheme is build upon an approximate spin-projection technique to represent the multireference low-spin ground state which extends the traditional description using broken-symmetry approaches or similar methods. Within this "extended broken-symmetry" (EBS) approach the total energy and the forces in the low-spin state are obtained as a particular weighted sum of the corresponding total energies and forces of the high-spin and broken-symmetry reference states which is achieved by an approximate spin-projection technique. Since this approach provides easy access to gradients, it allows for structure optimization and for the consistent

calculation of the exchange coupling constant J, at no additional cost, using the same spin-projection approximation for both calculations.

Most importantly, the proposed framework opens the doorway for an efficient implementation of ab initio molecular dynamics by propagating simultaneously two unrestricted Kohn−Sham determinants using Car−Parrinello techniques. The approach rests on theoretically solid ground as long as the system can be described by means of the Heisenberg spin Hamiltonian. The method is general, and the present implementation can be improved both systematically and consistently by using more sophisticated spin-projection approximations to eliminate the spin contaminations of the two Kohn−Sham reference determinants and by employing a better density functional based representation of these states.

To assess the value of the new scheme, it was compared to single-determinant treatments using a relevant but small binuclear iron−sulfur test system, the $[Fe_2S_2(SH)_4]^{2-}$ complex at 300 K in vacuo. In particular, the more compact Fe_2S_2 core leads to a $|J|$ value that is larger by about 10−15% in the EBS case. An interesting finding is the sensitivity of the minimum energy structure and thus of J on the approximation to the orbital overlap, i.e. the value of the overlap integrals, which establishes a unified connection of the outlined method to various schemes that can be found in the literature. From a very pragmatic point of view this dependence would offer the possibility to "fine tune" the structure of the system and thus $|J|$. However, it is clearly recommended to improve the underlying approximations (to the spin-projection and/or the representation of the reference states, see above) consistently within the general framework instead.

The present method allows one to carry out efficiently ab initio molecular dynamics simulations of antiferromagnetically coupled binuclear complexes within a two-determinant Car−Parrinello scheme. Analyzing trajectories obtained at room temperature it turns out that thermal fluctuations are able to change J by as much as about 50% with respect to the corresponding average value at 300 K. Since J is generated at no extra cost "on the fly" along the molecular dynamics trajectory, one can access readily its spectrum (or "density of states"), $A_{JJ}(\omega)$, by virtue of Fourier transforming its time-dependent evolution, $J(t)$. For the simple $[Fe_2S_2(SH)_4]^{2-}$ complex in vacuo the resulting power spectrum of J consists of two major peaks around 150 and 350 cm^{-1}, which can be understood in terms of two symmetry-adapted vibrational modes, $A_{g,A}$ and $A_{g,D}$, of the Fe_2S_2 core. This is to be expected qualitatively since J is known to depend sensitively on the distance between the metal cations and the bridging anions as well as on the bonding angle. But the present technique allows one to go beyond these qualitative rules in more complex situations, e.g., when environmental motion couples to the dynamics of the magnetic core as demonstrated in ref 41.

In the present study, the method has been assessed in much detail using a minimal model in vacuo. Clearly, for such a simple case more traditional methods such as harmonic analysis followed by evaluation of J along selected eigenvector displacements can be used to unravel the magneto-structural properties. At the same time it is evident that the method introduced can be used "as is" for much larger molecular systems, i.e. those which are accessible by present day density functional methods, where many coupled modes might be relevant for J thus rendering approaches difficult to apply where *all* relevant modes have to be identified a priori. Furthermore, the presented technique can be combined with suitable QM/MM coupling schemes to include extended environments via standard force field descriptions as demonstrated in ref 41. The potential of such an approach has been illustrated recently by studying the rather complex dynamical magnetostructural properties of the binuclear iron−sulfur cofactor in fully solvated ferredoxin from cyanobacterium *Anabaena* PCC7119. This investigation[41] uncovered that valuable information is encoded in the dynamics of the exchange coupling, $J(t)$, which can be analyzed conveniently when Fourier transformed into the corresponding spectrum $A_{JJ}(\omega)$. As suggested in ref 41 there is hope that experimental methods will be developed to follow the theoretical advances in this emerging field of dynamical magnetostructural properties.

Acknowledgment. We are grateful to Christian Boehme, Gerald Mathias, and Bernd Meyer for fruitful discussions and technical help. This work was supported in part by Deutsche Forschungsgemeinschaft (DFG) via grant MA 1547/7 and Fonds der Chemischen Industrie (FCI). The calculations were carried out using resources of Rechnerverbund-NRW, BOVILAB@RUB, and NIC.

Note Added after ASAP Publication. This article was released ASAP on June 26, 2008 with a minor error in the Acknowledgment. The correct version was posted on August 12, 2008.

References

(1) Noodleman, L.; Peng, C. Y.; Case, D. A.; Mouesca, J.-M. *Coord. Chem. Rev.* **1995**, *144*, 199–244.

(2) Lovell, T.; Himo, F.; Han, W.-G.; Noodleman, L. *Coord. Chem. Rev.* **2003**, *238* (239), 211–232.

(3) Yamanaka, S.; Yamaguchi, K. *Bull. Chem. Soc. Jpn.* **2004**, *77*, 1269–1286.

(4) Ciofini, I.; Daul, C. A. *Coord. Chem. Rev.* **2003**, *238* (239), 187−209.

(5) Calzado, C. J.; Cabrero, J.; Malrieu, J. P.; Caballol, R. *J. Chem. Phys.* **2002**, *116*, 2728–2747.

(6) Calzado, C. J.; Cabrero, J.; Malrieu, J. P.; Caballol, R. *J. Chem. Phys.* **2002**, *116*, 3985–4000.

(7) de Graaf, C.; Sousa, C.; de Moreira, P. R. I.; Illas, F. *J. Phys. Chem. A* **2001**, *105*, 11371–11378.

(8) Fink, K.; Fink, R.; Staemmler, V. *Inorg. Chem.* **1994**, *33*, 6219–6229.

(9) Broer, R.; Hozoi, L.; Nieuwpoort, W. C. *Mol. Phys.* **2003**, *101*, 233–240.

(10) Beinert, H.; Holm, R. H.; Münck, E. *Science* **1997**, *277*, 653–659.

(11) Rees, D. C. *Annu. Rev. Biochem.* **2002**, *71*, 221–246.

(12) Rees, D. C.; Howard, J. B. *Science* **2003**, *300*, 929–931.

(13) Johnson, D. C.; Dean, D. R.; Smith, A. D.; Johnson, M. K. *Annu. Rev. Biochem.* **2005**, *74*, 247–281.

(14) Palmer, G.; Dunham, W. R.; Fee, J. A.; Sands, R. H.; Iizuka, T.; Yonetani, T. *Biochim. Biophys. Acta* **1971**, *245*, 201–207.

(15) Sands, R. H.; Dunham, W. R. *Q. Rev. Biophys.* **1975**, *7*, 443–504.

(16) Kramers, H. A. *Physica* **1934**, *1*, 182–192.

(17) Anderson, P. W. *Phys. Rev.* **1950**, *79*, 350–356.

(18) Anderson, P. W. *Phys. Rev.* **1959**, *115*, 2–13.

(19) Kahn, O. *Molecular Magnetism*; VCH Publishers, Inc.: New York, 1993; pp 145−183.

(20) Hay, P. J.; Thibeault, J. C.; Hoffmann, R. *J. Am. Chem. Soc.* **1975**, *97*, 4884–4899.

(21) Neese, F. *J. Phys. Chem. Solids* **2004**, *65*, 781–785.

(22) Kahn, O.; Briat, B. *J. Chem. Soc. Faraday Trans. 2* **1976**, *72*, 268–281.

(23) Wang, C.; Fink, K.; Staemmler, V. *Chem. Phys.* **1995**, *201*, 87–94.

(24) Szabo, A.; Ostlund, N. S. *Modern Quantum Chemistry: Introduction to Advanced Electronic Structure Theory*; Dover Publications, Inc.: New York, 1996; pp 39−107.

(25) Adamo, C.; Barone, V.; Bencini, A.; Broer, R.; Filatov, M.; Harrison, N. M.; Illas, F.; Malrieu, J. P.; de Moreira, P. R. I. *J. Chem. Phys.* **2006**, *124*, 107101.

(26) Hübner, O.; Sauer, J. *J. Chem. Phys.* **2002**, *116*, 617–628.

(27) Mayer, I. *Adv. Quantum Chem.* **1980**, *12*, 189–262.

(28) Mayer, I.; Angelov, S. A. *Int. J. Quantum Chem.* **1980**, *18*, 783–796.

(29) Yamaguchi, K.; Yoshioka, Y.; Takatsuka, T.; Fueno, T. *Theor. Chim. Acta* **1978**, *48*, 185–206.

(30) Noodleman, L. *J. Chem. Phys.* **1981**, *74*, 5737–5743.

(31) Shoji, M.; Nishiyama, Y.; Maruno, Y.; Koizumi, K.; Kitagawa, Y.; Yamanaka, S.; Kawakami, T.; Okumura, M.; Yamaguchi, K. *Int. J. Quantum Chem.* **2004**, *100*, 887–906.

(32) Yamaguchi, K.; Jensen, F.; Dorigo, A.; Houk, K. N. *Chem. Phys. Lett.* **1988**, *149*, 537–542.

(33) Caballol, R.; Castell, O.; Illas, F.; de, P. R.; Moreira, I.; Malrieu, J. P. *J. Phys. Chem. A* **1997**, *101*, 7860–7866.

(34) Noodleman, L.; Lovell, T.; Liu, T.; Himo, F.; Torres, R. A. *Curr. Opin. Chem. Biol.* **2002**, *6*, 259–273.

(35) Hübner, O.; Sauer, J. *Phys. Chem. Chem. Phys.* **2002**, *4*, 5234–5243.

(36) Shoji, M.; Koizumi, K.; Kitagawa, Y.; Yamanaka, S.; Okumura, T. K. M.; Yamaguchi, K. *Int. J. Quantum Chem.* **2005**, *105*, 628–644.

(37) Shoji, M.; Koizumi, K.; Kitagawa, Y.; Yamanaka, S.; Okumura, M.; Yamaguchi, K. *Int. J. Quantum Chem.* **2007**, *107*, 609–627.

(38) Goodenough, J. B. *J. Phys. Chem. Solids* **1958**, *6*, 287–297.

(39) Kanamori, J. *J. Phys. Chem. Solids* **1959**, *10*, 87–98.

(40) Ginsberg, A. P. *Inorg. Chim. Acta Rev.* **1971**, *5*, 45–68.

(41) Schreiner, E.; Nair, N. N.; Pollet, R.; Staemmler, V.; Marx, D. *Proc. Natl. Acad. Sci.* **2007**, *104*, 20725–20730.

(42) Heisenberg, W. *Z. Phys.* **1928**, *49*, 619–636.

(43) Dirac, P. A. M. *Proc. Roy. Soc. A.* **1929**, *123*, 714–733.

(44) van Vleck, J. H. *The Theory of Electric and Magnetic Susceptibilities*, 1st ed.; Oxford University Press: London, United Kingdom, 1932; pp 316−360.

(45) Note: there is a obvious typographical error in the corresponding equation, eq 1, of ref 41.

(46) Yamaguchi, K.; Fukui, H.; Fueno, T. *Chem. Lett.* **1986**, 625–628.

(47) Nishino, M.; Yamanaka, S.; Yoshioka, Y.; Yamaguchi, K. *J. Phys. Chem. A* **1997**, *101*, 705–712.

(48) Löwdin, P. O. *Phys. Rev.* **1955**, *97*, 1474–1489.

(49) Wang, J.; Becke, A. D., Jr *J. Chem. Phys.* **1995**, *102*, 3477–3480.

(50) Cohen, A. J.; Tozer, D. J.; Handy, N. C. *J. Chem. Phys.* **2007**, *126*, 214104.

(51) Theophilou, I.; Thanos, S.; Theophilou, A. K. *J. Chem. Phys.* **2007**, *127*, 234103.

(52) Filatov, M.; Shaik, S. *Chem. Phys. Lett.* **1998**, *288*, 689–697.

(53) Filatov, M.; Shaik, S. *Chem. Phys. Lett.* **1999**, *304*, 429–437.

(54) de Moreira, P. R. I.; Costa, R.; Filatov, M.; Illas, F. *J. Chem. Theory Comput.* **2007**, *3*, 764–774.

(55) Ruiz, E.; Cano, J.; Alvarez, S.; Alemany, P. *J. Comput. Chem.* **1999**, *20*, 1391–1400.

(56) Car, R.; Parrinello, M. *Phys. Rev. Lett.* **1985**, *55*, 2471–2474.

(57) Marx, D.; Hutter, J. In *Modern Methods and Algorithms of Quantum Chemistry*; Grotendorst, J., Ed.; John von Neumann Institute for Computing (NIC): Forschungszentrum Jülich, Germany, 2000; *3*, pp 301−449.

(58) Norman, J. G.; Ryan, P. B.; Noodleman, L. *J. Am. Chem. Soc.* **1980**, *102*, 4279–4282.

(59) Cory, M. G.; Stavrev, K. K.; Zerner, M. C. *Int. J. Quantum Chem.* **1997**, *63*, 781–795.

(60) CPMD, Version 3.11, Copyright IBM Corp. 1990−2008, MPI für Festkörperforschung Stuttgart, 1997−2001.

(61) Perdew, J. P.; Burke, K.; Ernzerhof, M. *Phys. Rev. Lett.* **1996**, *77*, 3865–3868.

(62) Perdew, J. P.; Burke, K.; Ernzerhof, M. *Phys. Rev. Lett.* **1997**, *78*, 1396–1396.

(63) Vanderbilt, D. *Phys. Rev. B* **1990**, *41*, 7892–7895.

(64) Martyna, G. J.; Tuckerman, M. E. *J. Chem. Phys.* **1999**, *110*, 2810–2821.

(65) Martyna, G. J.; Klein, M. L.; Tuckerman, M. *J. Chem. Phys.* **1992**, *97*, 2635–2643.

(66) Sigfridsson, E.; Olsson, M. H. M.; Ryde, U. *Inorg. Chem.* **2001**, *40*, 2509–2519.

(67) Gillum, W. O.; Frankel, R. B.; Foner, S.; Holm, R. H. *Inorg. Chem.* **1976**, *15*, 1095–1100.

(68) Cabrero, J.; Calzado, C. J.; Maynau, D.; Caballol, R.; Malrieu, J. P. *J. Phys. Chem. A* **2002**, *106*, 8146–8155.

(69) Martin, R. L.; Illas, F. *Phys. Rev. Lett.* **1997**, *79*, 1539–1542.

(70) Ruiz, E.; Alvarez, S.; Cano, J.; Polo, V. *J. Chem. Phys.* **2005**, *123*, 164110.

(71) Perdew, J. P.; Zunger, A. *Phys. Rev. B* **1981**, *23*, 5048–5079.

(72) Akande, A.; Sanvito, S. *J. Chem. Phys.* **2007**, *127*, 034112.

(73) d'Avezac, M.; Calandra, M.; Mauri, F. *Phys. Rev. B* **2005**, *71*, 205210.

(74) VandeVondele, J.; Sprik, M. *Phys. Chem. Chem. Phys.* **2005**, *7*, 1363–1367.

(75) Tavernelli, I. *J. Phys. Chem. A* **2007**, *111*, 13528–13536.

(76) Anisimov, V. I.; Zaanen, J.; Andersen, O. K. *Phys. Rev. B* **1991**, *44*, 943–954.

(77) Liechtenstein, A. I.; Anisimov, V. I.; Zaanen, J. *Phys. Rev. B* **1995**, *52*, R5467–R5470.

(78) Rohrbach, A.; Hafner, J.; Kresse, G. *J. Phys.: Condens. Matter* **2003**, *15*, 979–996.

(79) Kulik, H. J.; Cococcioni, M.; Scherlis, D. A.; Marzari, N. *Phys. Rev. Lett.* **2006**, *97*, 103001.

(80) Sit, P. H.-L.; Cococcioni, M.; Marzari, N. *J. Electroanal. Chem.* **2007**, *607*, 107–112.

(81) Dederichs, P. H.; Blügel, S.; Zeller, R.; Akai, H. *Phys. Rev. Lett.* **1984**, *53*, 2512–2515.

(82) Rudra, I.; Wu, Q.; van Voorhis, T. *J. Chem. Phys.* **2006**, *124*, 024103.

(83) Rudra, I.; Wu, Q.; van Voorhis, T. *Inorg. Chem.* **2007**, *46*, 10539–10548.

(84) Herrmann, C.; Yu, L.; Reiher, M. *J. Comput. Chem.* **2006**, *27*, 1223–1239.

(85) Ramírez, R.; López-Ciudad, T. P.; Kumar, P.; Marx, D. *J. Chem. Phys.* **2004**, *121*, 3973–3983.

(86) Leach, A. R. *Molecular modelling: principles and applications*, 2nd ed.; Pearson Education Limited: Harlow, United Kingdom, 2001; pp 458−508.

(87) Schreiner, E. Biochemical Aspects of Iron-Sulfur Systems: Magnetostructural Properties of Ferredoxins and Prebiotic Peptide Synthesis Involving Pyrite, Ph.D. Thesis, Ruhr-Universität Bochum, Germany, 2007.

CT800089X